CHEMISTRY
AN ASIAN JOURNAL
ACES
FULL PAPER

DOI: 10.1002/asia.201300165

Alkane Oxidation by an Immobilized Nickel Complex Catalyst: Structural and Reactivity Differences Induced by Surface-Ligand Density on Mesoporous Silica

Jun Nakazawa,*[a] Tomoaki Hori,[a] T. Daniel P. Stack,[b] and Shiro Hikichi*[a]

Abstract: Immobilized nickel catalysts SBA*-**L**-x/Ni (**L** = bis(2-pyridylmethyl)(1H-1,2,3-triazol-4-ylmethyl)amine) with various ligand densities (**L** content (x) = 0.5, 1, 2, 4 mol% Si) have been prepared from azidopropyl-functionalized mesoporous silicas SBA-N_3-x. Related homogeneous ligand $\mathbf{L}^{t\mathrm{Bu}}$ and its Ni^{II} complexes, $[Ni(\mathbf{L}^{t\mathrm{Bu}})(OAc)_2(H_2O)]$ ($\mathbf{L}^{t\mathrm{Bu}}$/Ni) and $[Ni(\mathbf{L}^{t\mathrm{Bu}})_2]BF_4$ (2 $\mathbf{L}^{t\mathrm{Bu}}$/Ni), have been synthesized. The **L**/Ni ratio (0.9–1.7:1) in SBA*-**L**-x/Ni suggests the formation of an inert $[Ni\mathbf{L}_2]$ site on the surface at higher ligand loadings. SBA*-**L**-x/Ni has been applied to the catalytic oxidation of cyclohexane with *m*-chloroperbenzoic acid (*m*CPBA). The catalyst with the lowest loading shows high activity in its initial use as the homogeneous $\mathbf{L}^{t\mathrm{Bu}}$/Ni catalyst, with some metal leaching. As the ligand loading increases, the activity and Ni leaching are suppressed. The importance of site-density control for the development of immobilized catalysts has been demonstrated.

Keywords: heterogeneous catalysis · immobilization · mesoporous materials · nickel · oxidation

Introduction

Homogeneous metal catalysts hold great promise for changing the chemo- and regioselectivities in fine-chemical transformations through simple ligand variation. The efficient and well-defined immobilization of such catalysts on solid supports provides additional advantages, such as facile separation, reusability, and catalyst site-isolation.[1] However, the translation of catalytic reactivity from a homogeneous catalyst to a heterogenized analogue is often associated with a decrease in activity, presumably owing to interactions of the catalyst with itself or with ligands on the support surface.[2] The ability to define the relevance of such interactions with respect to the catalysis would facilitate the use of heterogenized homogeneous catalysts. In fact, these interactions with surface ligands might even be exploited to yield new types of transformations, because site-isolation on the surface could prevent the formation of the most thermodynamically stable species, as is generally observed in a homogeneous solution.

It is now possible to immobilize a variety of useful discrete molecules at a defined level of loading on mesoporous silica solid supports, by using a two-step synthetic procedure that involves a copper(I)-catalyzed azide–alkyne cycloaddition reaction (CuAAC, also called a click reaction).[3] The first step is the direct incorporation of a defined quantity of an azide (e.g., 3-azidopropyltriethoxysilane) into the synthesis of a material that exploits the discotic mesophase of nonionic surfactant Pluronic P-123 under acidic conditions and the hydrolysis of tetraethylorthosilicate; this method is referred to as a direct synthesis, in which the organic azide groups are preferentially oriented into the templated pores once the surfactant is removed under soft conditions.[4] Beyond providing control over the azide loading, the material retains the advantageous properties of the original SBA-15 mesoporous silica,[5] such as mechanical strength, which results from the thick silica walls, and large surface areas, which are accessible through well-defined mesopores. The covalent attachment of ethynylated molecules onto the azidopropyl tethers, as the second step in the synthetic procedure, relies on the highly selective, high-yielding click reaction that is widely applied in many research areas.[6] This procedure not only provides reproducible attachment with desired surface coverage, but also randomly distributed functional groups on the solid surface. The use of these materials enables the investigation of the interactions between surface-immobilized functionalities, with special focus on the effects of metal-complex sites on the coordination structure and catalytic reactivity through interactions between immobilized ligands.

In 2006, Itoh and co-workers reported that $[Ni^{2+}(tpa)]$ (tpa = tris(2-pyridylmethyl)amine) complexes efficiently catalyzed the oxidation of alkanes with *m*-chloroperbenzoic acid (*m*CPBA) with high alcohol selectivity (Scheme 1).[7]

---

[a] Dr. J. Nakazawa, T. Hori, Prof. Dr. S. Hikichi
Department of Material and Life Chemistry
Kanagawa University
Yokohama, Kanagawa 221-8686 (Japan)
Fax: (+81) 45-413-9770
E-mail: jnaka@kanagawa-u.ac.jp

[b] Prof. Dr. T. D. P. Stack
Department of Chemistry
Stanford University
Stanford, CA, 94305-5080 (USA)

Herein, we compare the homogeneous and heterogeneous reactivities of a related nickel complex with the *N,N*-bis(2-pyridylmethyl)-*N*-{(1H-1,2,3-triazol-4-yl)methyl}amine (**L**) ligand. This ligand is readily prepared and covalently attached onto azide-functionalized SBA-15 by using CuAAC reactions with various surface-ligand densities. The coordination of the surface-immobilized nickel complex was inferred by comparison with homogeneous analogues. A comparison of the oxidation of cyclohexane with *m*CPBA and both the homogeneous and immobilized nickel complexes provides insights into the nature of the active catalytic species.

Results and Discussion

Preparation and Characterization of the Homogeneous Complexes

N,N-Bis(2-pyridylmethyl)-*N*-{(1-*tert*-butyl-1H-1,2,3-triazol-4-yl)methyl}amine ($\mathbf{L}^{t\mathbf{Bu}}$) was prepared from *N*-propargyl-*N,N*-bis(2-pyridiylmethyl)amine (**1**)[6j–l] and *tert*-butylazide[8] by using a click reaction (Scheme 2) as a homogeneous analogue to evaluate the effect of triazole substitution of one of the pyridine arms on the tpa ligand. The facile preparation of ligands with potentially coordinating triazole groups is called the "click-to-chelate" approach.[6p,9] Compound $\mathbf{L}^{t\mathbf{Bu}}$ was fully characterized (elemental analysis, MS (ESI), and IR, UV/Vis, and NMR (^{1}H, ^{13}C) spectroscopy). The mixture of equimolar amounts of $\mathbf{L}^{t\mathbf{Bu}}$ and Ni^{II} acetate give [Ni^{2+}(OAc)$_2$(H$_2$O)($\mathbf{L}^{t\mathbf{Bu}}$)], (= $\mathbf{L}^{t\mathbf{Bu}}$/Ni) as blue crystals, whilst the addition of an excess of the ligand to nickel acetate also gave $\mathbf{L}^{t\mathbf{Bu}}$/Ni in quantitative yield. In contrast, the addition of $Ni(BF_4)\cdot 6H_2O$, which had a noncoordinating counter anion, to two equivalents of the ligand in EtOH afforded purple crystals of [Ni($\mathbf{L}^{t\mathbf{Bu}}$)$_2$](BF$_4$)$_2$ (2$\mathbf{L}^{t\mathbf{Bu}}$/Ni). Both nickel complexes ($\mathbf{L}^{t\mathbf{Bu}}$/Ni and 2$\mathbf{L}^{t\mathbf{Bu}}$/Ni) were fully characterized by elemental analysis, MS (ESI), IR and UV/Vis spectroscopy, and X-ray crystallography.

The molecular structures of compounds $\mathbf{L}^{t\mathbf{Bu}}$/Ni and 2$\mathbf{L}^{t\mathbf{Bu}}$/Ni, as obtained by X-ray crystallographic analysis, are shown in Figure 1 and Figure 2 and selected bond lengths and angles are collected in Table 1 and Table 2, respectively.

Abstract in Japanese:

ビスピリジルメチルアミン配位子 **L** の担持量 (*x*) を制御した固定化錯体触媒 SBA*-**L**-*x*/Ni を調製し，その均一系モデル錯体 [Ni($\mathbf{L}^{t\mathbf{Bu}}$)(OAc)$_2$(OH$_2$)] ($\mathbf{L}^{t\mathbf{Bu}}$/Ni) および [Ni($\mathbf{L}^{t\mathbf{Bu}}$)$_2$](BF$_4$)$_2$ についても合成・構造決定した．固定化錯体の **L**/M 比率より，配位子担持量の増加に伴って担体上の錯体種が [Ni**L**(X)$_n$] から [Ni**L**$_2$] へ変化することが示唆された．*m*CPBA を酸化剤とするシクロヘキサンの酸化反応に対して，均一および固定化錯体触媒の活性を評価した．$\mathbf{L}^{t\mathbf{Bu}}$/Ni は既報の tpa/Ni 錯体と同様の高い活性を示した．一方固定化錯体触媒は配位子担持量の増大に伴い活性が低下した．この結果は担体上における配位子量が錯体種の構造および反応活性を制御する上で重要な要素であることを示している．

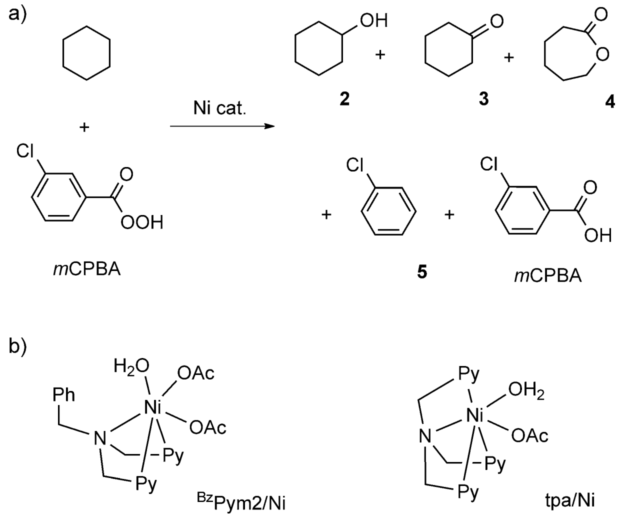

Scheme 1. a) Nickel-catalyzed oxidation of cyclohexane with *m*CPBA. b) Reported Ni catalysts for the oxidation reactions.

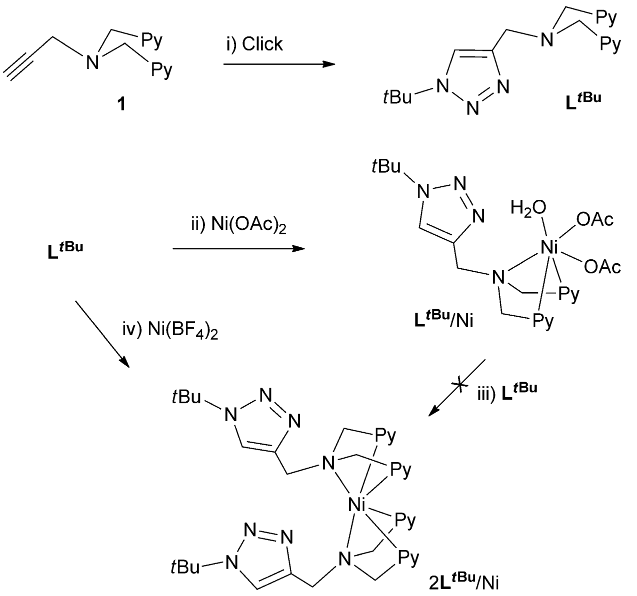

Scheme 2. Preparation of $\mathbf{L}^{t\mathbf{Bu}}$ and its nickel(II) complexes, $\mathbf{L}^{t\mathbf{Bu}}$/Ni and 2$\mathbf{L}^{t\mathbf{Bu}}$/Ni. Reaction conditions: (i) *tert*-butylazide, Cu^0 powder, N$_2$, RT, 24 h; (ii) $Ni(OAc)_2\cdot 4H_2O$, MeOH, 30 min; (iii) $\mathbf{L}^{t\mathbf{Bu}}$ (2 equiv), MeOH, 30 min; (iv) $Ni(BF_4)_2\cdot 6H_2O$, EtOH, 30 min.

Two independent isomers with similar geometries around the nickel ions existed in the unit cells of both complexes. Both [Ni**L**(X)$_n$] (X = solvent, anion, etc.) and [Ni**L**$_2$]-type structures were also reported with the *N,N*-bis(2-pyridylmethyl)benzylamine ligand (^{Bz}Pym2 or BzBPA in reference compounds).[7b,10] In $\mathbf{L}^{t\mathbf{Bu}}$/Ni, the triazole group does not coordinate to the Ni center (Ni–N > 5 Å). The coordination environment (two pyridine groups, a tertiary amine, a water molecule, and two monodentate acetate groups) is more similar to that in [Ni^{2+}(^{Bz}Pym2)(OAc)$_2$(H$_2$O)] (^{Bz}Pym2/Ni)[7b] than in [Ni(tpa)(OAc)(H$_2$O)] (tpa/Ni).[7a] The nitrogen donor atoms (N1, N2, N3) of the bis(2-pyridylmethyl)amine)

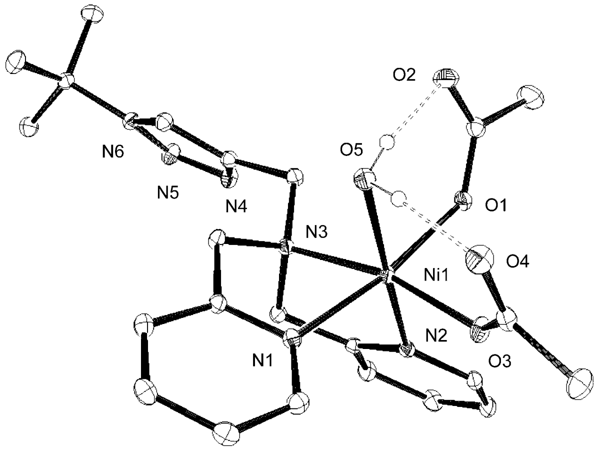

Figure 1. Molecular structure of complex $\mathbf{L}^{t\mathrm{Bu}}$/Ni (unit 1). Two independent isomers exist in the unit cell. Ellipsoids are set at 30% probability; hydrogen atoms on carbon atoms are omitted for clarity.

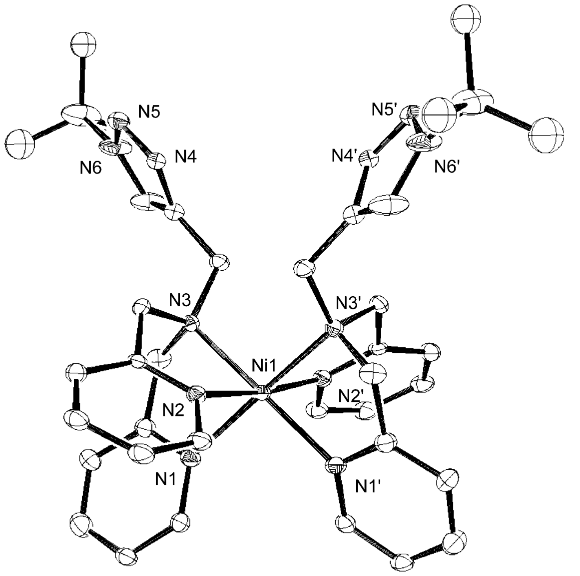

Figure 2. Molecular structure of complex 2$\mathbf{L}^{t\mathrm{Bu}}$/Ni (unit 1). Two independent isomers exist in the unit cell. Ellipsoids are set at 30% probability; hydrogen atoms on carbon atoms are omitted for clarity.

Table 1. Selected bond lengths [Å] and angles [°] in the single crystal of complex $\mathbf{L}^{t\mathrm{Bu}}$/Ni.[a]

	Unit 1	Unit 2
Ni1(2)–N1(7)	2.102(2)	2.094(2)
Ni1(2)–N2(8)	2.060(2)	2.061(2)
Ni1(2)–N3(9)	2.164(2)	2.153(2)
Ni1(2)–O1(6)	2.080(2)	2.075(2)
Ni1(2)–O3(8)	2.031(2)	2.039(2)
Ni1(2)–O5(10)	2.099(2)	2.097(2)
O2(7)–O5(10)	2.639(2)	2.638(3)
O4(9)–O5(10)	2.679(3)	2.633(2)
N1(7)-Ni1(2)-N2(8)	99.99(7)	97.78(7)
N1(7)-Ni1(2)-N3(9)	78.02(7)	78.07(7)
N1(7)-Ni1(2)-O1(6)	171.47(7)	173.94(7)
N1(7)-Ni1(2)-O3(8)	93.54(7)	94.75(7)
N1(7)-Ni1(2)-O5(10)	84.79(7)	87.19(7)
N2(8)-Ni1(2)-N3(9)	81.64(7)	81.51(7)
N2(8)-Ni1(2)-O1(6)	84.71(7)	83.65(7)
N2(8)-Ni1(2)-O3(8)	89.99(7)	94.13(7)
N2(8)-Ni1(2)-O5(10)	173.28(7)	170.70(7)
N3(9)-Ni1(2)-O1(6)	95.77(7)	96.37(7)
N3(9)-Ni1(2)-O3(8)	166.81(7)	170.92(7)
N3(9)-Ni1(2)-O5(10)	94.85(7)	91.91(6)
O1(6)-Ni1(2)-O3(8)	93.56(7)	91.01(7)
O1(6)-Ni1(2)-O5(10)	89.97(7)	90.60(7)
O3(8)-Ni1(2)-O5(10)	94.45(7)	93.27(6)

[a] Atom numbering in unit 2 is shown in parentheses.

Table 2. Selected bond lengths [Å] and angles [°] in the single crystal of complex 2$\mathbf{L}^{t\mathrm{Bu}}$/Ni.[a]

	Unit 1	Unit 2
Ni1(2)–N1(7)	2.122(4)	2.118(3)
Ni1(2)–N2(8)	2.046(3)	2.044(3)
Ni1(2)–N3(9)	2.165(3)	2.181(3)
N1(7)-Ni1(2)-N2(8)	82.3(1)	82.5(1)
N1(7)-Ni1(2)-N3(9)	79.6(1)	79.7(1)
N1(7)-Ni1(2)-N1′(7′)	98.1(1)	97.9(1)
N1(7)-Ni1(2)-N2′(8′)	102.6(1)	102.7(1)
N1(7)-Ni1(2)-N3′(9′)	173.6(1)	173.8(1)
N2(8)-Ni1(2)-N3(9)	83.1(1)	82.6(1)
N2(8)-Ni1(2)-N2′(8′)	172.7(1)	172.2(1)
N2(8)-Ni1(2)-N3′(9′)	92.3(1)	92.5(1)
N3(9)-Ni1(2)-N3′(9′)	103.2(1)	103.4(1)

[a] Atom numbering in unit 2 is shown in parentheses.

unit occupy slightly distorted *facial* positions in the octahedral geometry and the water donor atom (O5) occupies a position *trans* to one of the pyridine donor groups (N2). The Ni–N(pyridine) (N1, N2) bond lengths are shorter than the Ni–N(tertiary amine) bond (N3 = 2.164 Å). In addition, the following differences in the bond lengths, which are derived from the donating character of the *trans*-locating ligand, have been observed: 1) In the two pyridine groups, the Ni–N distance to the pyridine donor (N1 = 2.102 Å) that is located *trans* to an acetate group (O1) is longer than that of the other pyridine group (N2 = 2.060 Å), which is *trans* to the water molecule (O5). 2) In terms of the Ni–O distances, the distance to the acetate group (O3 = 2.031 Å) that is located *trans* to the tertiary amine is shorter than that to the other acetate group (O1 = 2.080 Å) or the water molecule (O5 = 2.099 Å), which are located *trans* to the pyridine groups.

In the molecular structure of complex 2$\mathbf{L}^{t\mathrm{Bu}}$/Ni, the nickel ion is located on a two-fold axis and two symmetrically equivalent molecules of the $\mathbf{L}^{t\mathrm{Bu}}$ ligand occupy the octahedral coordination environment of the nickel. Each ligand is coordinated in a *facial* and tridentate manner by two pyridine groups and a tertiary amine moiety. The two tertiary amine sites (N3, N3′) on the nickel atom occupy *cis* positions. The Ni–N(pyridine) bond lengths (N1 = 2.122 Å, N2 = 2.046 Å) are shorter than that of the Ni–N(tertiary amine) bond (N3 = 2.165 Å). Although there have been some very recent reports of coordination structures between tightly coordinating triazole groups and various metal ions,[9] the triazole group in $\mathbf{L}^{t\mathrm{Bu}}$ is not coordinated to the Ni center in this complex. The chelate geometry of the triazolylmethyl arm in $\mathbf{L}^{t\mathrm{Bu}}$ could be unsuitable for coordination, especially for the nickel-coordination environment.

Preparation and Characterization of the Immobilized Nickel Complexes

The immobilized catalysts were prepared as shown in Scheme 3. Azidopropyl-functionalized mesoporous silica with controlled azide loadings, SBA-N_3-x (x = molar content of $(EtO)_3Si(CH_2)_3N_3$ in the silica preparation; 0.5, 1, 2, 4 mol% Si), was synthesized according to a literature procedure.[3] The click attachment of ligand precursor **1** onto the SBA-N_3-x support was also performed under the same conditions, by using $CuSO_4$/sodium ascorbate in DMF to afford the ligand-immobilized silicas (SBA-**L**-x). The progress of the click reaction was monitored by the decrease (>70%) in the intensity of the azide peak (at 2110 cm^{-1}) in the IR spectra. A stoichiometric amount of the copper catalyst was required for the click immobilization, in contrast to the standard homogeneous-phase conditions (about 5 mol% Cu), because the copper intermediate was captured by the in situ generated immobilized ligand site, which prevented its migration onto other surface azide sites. Excess copper ions were fully removed by washing with a solution of the chelating reagent (sodium N,N-diethyldithiocarbamate, Na-ddtc). To simplify the reactivity study, the surface Si–OH groups were end-capped by treatment with 1,1,1,3,3,3-hexamethyldisilazane (HMDS) in toluene to give ligand-immobilized, end-capped silica (SBA*-**L**-x). Then, the SBA*-**L**-x silicas were treated with a solution of nickel(II) acetate in MeOH to give the SBA*-**L**-x/Ni catalysts.

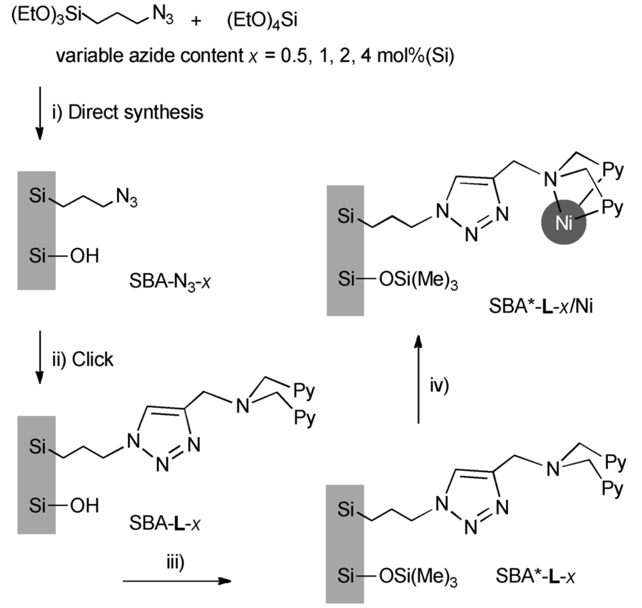

Scheme 3. Preparation of the heterogeneous SBA*-**L**-x/Ni catalysts. Reaction conditions: (i) P_{123} polymer, HCl, water, 35 °C 24 h, then 100 °C 24 h, then polymer removal on a Soxhlet apparatus, EtOH, 24 h; (ii) $CuSO_4{\cdot}5H_2O$, sodium ascorbate, DMF, N_2, 24 h, RT; (iii) HMDS, toluene 50 °C, 1 h; (iv) $Ni(OAc)_2{\cdot}4H_2O$, MeOH.

The physicochemical properties of the prepared silicas, as well as their nickel and ligand loadings, are summarized in Table 3. The surface area, pore volume, and pore diameter of the silica materials were calculated from their nitrogen-adsorption/desorption isotherms by using the Brunauer–Emmett–Teller (BET)[11] and Barrett–Joyner–Halenda (BJH) methods.[12] The nitrogen-adsorption isotherms of the SBA*-**L**-x materials at all loadings of SBA-**L**-x show a type-IV pattern, thus indicating that the mesoporous structure of the SBA-N_3-x material is maintained during the surface modification by the click and end-capping reactions.[3] As the loading (x) increases, the surface area, pore volume, and pore diameter decrease, owing to the occupation of the pore surface by the organic functionalities. The smooth access of small molecules to the metal-complex sites is even allowed in the mesopores of higher-loading samples, such as SBA-**L**-4 (and also SBA-**R**-8 in a previous report[3]). This accessibility was previously confirmed by the complete removal of the trapped copper catalyst from these materials by Na-ddtc during the preparation of the materials.

Table 3. Physicochemical properties of functionalized silicas.

Property	Silica	x			
		0.5	1	2	4
A [$m^2\,g^{-1}$][a]	SBA-**L**-x	685	724	498	430
	SBA*-**L**-x	590	602	422	302
V [$m^3\,g^{-1}$][b]	SBA-**L**-x	0.96	0.84	0.39	0.52
	SBA*-**L**-x	0.86	0.73	0.36	0.30
D [nm][c]	SBA-**L**-x	4.85	4.04	3.46	3.93
	SBA*-**L**-x	5.00	4.12	3.44	3.22
L loading [$mmol\,g^{-1}$][d]	SBA-**L**-x	0.08	0.11	0.25	0.32
	SBA*-**L**-x	0.07	0.12	0.25	0.33
Ni loading [$mmol\,g^{-1}$][e]	SBA*-**L**-x/Ni	0.08	0.14	0.22	0.19
	used[f]	0.03 (0.06)	0.05	0.14	0.18
	reused[f]	0.02 (0.05)	0.04	0.14	0.17
L/Ni ratio[g]		0.9	0.9	1.1	1.7

[a] BET surface area. [b] Pore volume (BJH method, desorption branch). [c] Pore diameter (BJH method, desorption branch). [d] Determined from the UV/Vis absorption spectrum after silica digestion. [e] Determined from the atomic absorption analysis after silica digestion. [f] Used and re-used catalysts from the oxidation reactions after washing with MeOH (CH_2Cl_2 in parentheses). [g] Calculated according to [**L** loading of SBA*-**L**-x]/[Ni loading of SBA*-**L**-x/Ni].

The ligand loading in SBA-**L**-x and SBA-**L***-x was quantified by UV/Vis spectrometry after silica digestion by treatment with OH^- and F^-, respectively. The ligand loading showed an almost-linear increase with the initial azide content (x) during the silica preparation. The nickel loading in the SBA-**L***-x/Ni materials was quantified by atomic absorption analysis after silica digestion by treatment with OH^-.

In contrast to the ligand loading, the nickel loading on the SBA*-**L**-x materials showed a different trend. The silica with the lowest ligand loading, SBA*-**L**-0.5, retained a similar amount of nickel ions to that of the loaded ligand ($\mathbf{L}=0.07$ and $\mathrm{Ni}=0.08\ \mathrm{mmol\,g^{-1}}$), whereas the silica with the highest ligand loading, SBA*-**L**-4, only retained roughly half of the amount of nickel as that of the ligand ($\mathbf{L}=0.32$ and $\mathrm{Ni}=0.19\ \mathrm{mmol\,g^{-1}}$).

To obtain further structural information on the immobilized nickel complexes, the UV/Vis absorption spectra of the SBA*-**L**-*x*/Ni materials were compared with those of their homogeneous analogues, $\mathbf{L}^{t\mathrm{Bu}}$/Ni and 2$\mathbf{L}^{t\mathrm{Bu}}$/Ni (Figure 3).[13]

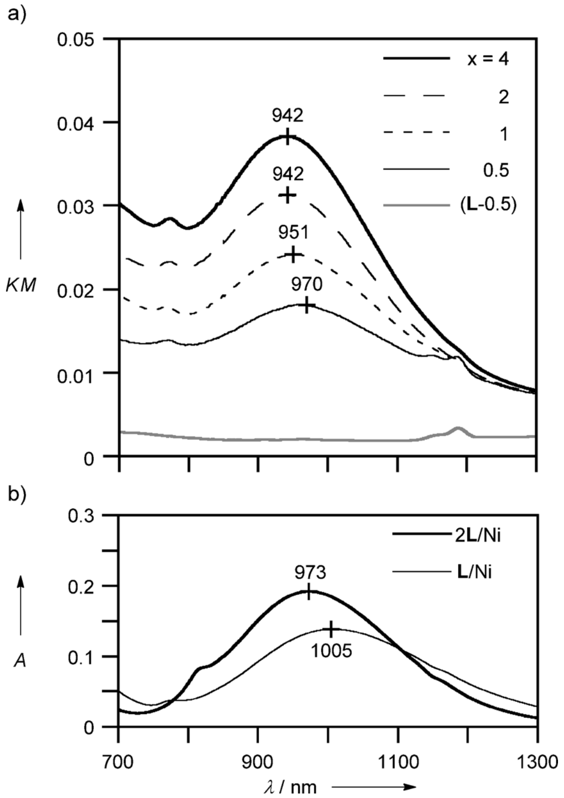

Figure 3. UV/Vis spectra of the nickel complexes. a) Solid-state diffusion reflectance spectra of immobilized metal complexes SBA*-**L**-*x*/Ni ($x=0.5$, 1, 2, 4), with SBA*-**L**-0.5 as a reference. b) UV/Vis spectra of homogeneous complexes $\mathbf{L}^{t\mathrm{Bu}}$/Ni and 2$\mathbf{L}^{t\mathrm{Bu}}$/Ni in CH_2Cl_2 (0.01 $\mathrm{mol\,dm^{-3}}$).

In CH_2Cl_2, the homogeneous $\mathbf{L}^{t\mathrm{Bu}}$/Ni complex shows a peak at 1005 nm ($\varepsilon=14\ \mathrm{mol^{-1}dm^3cm^{-1}}$), owing to a d–d band, which is similar to the reported values of $[\mathrm{Ni}(^{\mathrm{Bz}}\mathrm{Pym2})(\mathrm{OAc})_2(\mathrm{H_2O})]$ (1010 nm, $\varepsilon=13\ \mathrm{mol^{-1}dm^3cm^{-1}}$ in CH_2Cl_2) and $[\mathrm{Ni}(^{t\mathrm{Bu}}\mathrm{Pym2})(\mathrm{NO_3})_2]$ (979 nm, $\varepsilon=11\ \mathrm{mol^{-1}dm^3cm^{-1}}$ in MeCN).[7b,10] In contrast, the corresponding band of complex 2$\mathbf{L}^{t\mathrm{Bu}}$/Ni is observed at 973 nm ($\varepsilon=19\ \mathrm{mol^{-1}dm^3cm^{-1}}$), whereas that of $[\mathrm{Ni}(^{\mathrm{Bz}}\mathrm{Pym2})_2](\mathrm{ClO_4})_2$ is at 958 nm ($\varepsilon=16\ \mathrm{mol^{-1}dm^3cm^{-1}}$ in MeCN).[10] In our homogeneous complexes, the difference between the peak maxima of $\mathbf{L}^{t\mathrm{Bu}}$/Ni and 2$\mathbf{L}^{t\mathrm{Bu}}$/Ni is 32 nm. On the other hand, the immobilized nickel complexes, SBA*-**L**-*x*/Ni, also show a 28 nm peak shift of the d–d band in the solid-state diffusion reflectance spectra from 970 ($x=0.5$) to 942 nm ($x=4$) upon increasing the ligand loading. This similarity in the shifts of the homogeneous and heterogeneous cases suggests the formation of $[\mathrm{Ni}\mathbf{L}_2]$ species on the ligand-rich silica surface. It should be noted again that complex 2$\mathbf{L}^{t\mathrm{Bu}}$/Ni is not formed from $[\mathrm{Ni(OAc)_2}]$ in homogeneous solution. This result indicates that the coordination equilibrium of the second ligand leans toward the formation of $[\mathrm{Ni}\mathbf{L}_2]$ in the ligand-rich environment on the solid support.

Homogeneous Oxidation Catalysis

The homogeneous oxidation of cyclohexane by *m*CPBA in the presence of the $\mathbf{L}^{t\mathrm{Bu}}$/Ni catalyst was initially examined under literature conditions to compare the reactivity and reaction mechanisms with those of the tpa/Ni and $^{\mathrm{Bz}}$Pym2/Ni catalysts (Table 4, entries 1–3).[7] The yields of cyclohexanol (**2**), cyclohexanone (**3**), ε-caprolactone (**4**; as the Baeyer–Villiger reaction product from the reaction between compound **3** and *m*CPBA), and chlorobenzene (**5**; as an oxidant byproduct) were quantified by GC. The progress of product formation in the reaction with the $\mathbf{L}^{t\mathrm{Bu}}$/Ni catalyst indicates that the reaction is complete within 1 h, as in the tpa/Ni and $^{\mathrm{Bz}}$Pym2/Ni cases (Figure 4). The reactivity of the $\mathbf{L}^{t\mathrm{Bu}}$/Ni catalyst is closer to that of tpa/Ni than $^{\mathrm{Bz}}$Pym2/Ni in terms of two factors: 1) the catalyst turnover number (TON = [product]/[Ni]) and 2) the selectivity for alcohol **2** versus ketone **3**. The triazole group on the $\mathbf{L}^{t\mathrm{Bu}}$ ligand probably serves as a coordination donor or a base. Roughly half of the amount of chlorobenzene (**5**), as a byproduct from *m*CPBA, was detected, based on the sum of the cyclohexane-oxidation products. This result suggests that the reaction with the $\mathbf{L}^{t\mathrm{Bu}}$/Ni system may also proceed through a $\mathrm{Ni^{II}{-}O^{\bullet}}$ radical species, followed by *m*CPBA coordination and O–O homolysis, as suggested for the tpa/Ni system.[7] The following two experi-

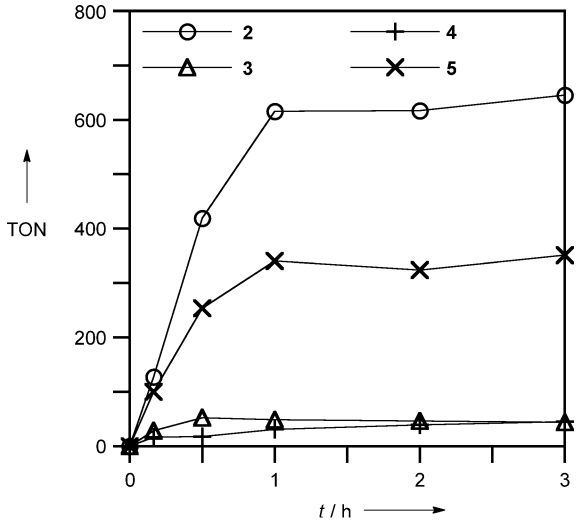

Figure 4. Progress of product formation in the oxidation of cyclohexane catalyzed by $\mathbf{L}^{t\mathrm{Bu}}$/Ni under standard conditions; cyclohexanol **2** (○), cyclohexanone **3** (△), ε-caprolactone **4** (+), and chlorobenzene **5** (X); (TON = [product]/[Ni]).

ments indicated that some of the active species survived under the original conditions (Table 4, entry 3): 1) The addition of an oxidant (2 mmol) into the reacted mixture (to entry 3) at 90 min induced a partial increase in the yield of the products. 2) Decreasing the amount of catalyst to 0.2 μmol caused the reaction rate to slow, but the final TON of compound **2** reached 3395 (Table 4, entry 4).

In the case of complex 2$\mathbf{L}^{t\mathrm{Bu}}$/Ni, the reaction afforded similar amounts of the products as in the case of $\mathbf{L}^{t\mathrm{Bu}}$/Ni after a longer period of time (2 h), thus suggesting that the reactive [Ni**L**(X)$_n$] species was supplied in situ by the dissociation equilibrium of one of the $\mathbf{L}^{t\mathrm{Bu}}$ ligands (Table 4, entry 6).

Heterogeneous Oxidation Catalysis

Heterogeneous catalysis with the SBA*-**L**-*x*/Ni materials was also performed under the same conditions (Table 4 and Figure 5). The SBA*-**L**-0.5/Ni catalyst exhibited a TON of 534 for compound **2** after 3 h with activity saturation, whilst homogeneous catalyst $\mathbf{L}^{t\mathrm{Bu}}$/Ni showed a TON of 616 for compound **2** (Table 4, entries 3 versus 7). A filtration test was performed to check whether the catalysis occurred on the immobilized complex or on the leached metal ions.[1g,14] Under the standard conditions, with the SBA*-**L**-0.5/Ni catalyst, the reaction mixture was passed through a syringe filter (ADVANTEC DISMIC-13 PTFE 0.2 μm) under an Ar atmosphere for 1 h. GC analysis of the eluent showed no further increase in the yield of the products, thus suggesting that the oxidation was only catalyzed by the immobilized nickel complex. Nam et al. also reported that Ni(ClO_4) showed no catalytic activity for the oxidation of alkanes with *m*CPBA.[15]

Table 4. Catalyzed oxidation of cyclohexane with *m*CPBA as an oxidant.[a]

Entry	Catalyst	*t* [h]	TON **2**	 **3**	 **4**	 **5**	 **2**/(**3**+**4**)
1	tpa/Ni[b]	1	587	69	–	–	8.5
2	$^{\mathrm{Bz}}$Pym2/Ni[b]	1	455	69	–	–	6.6
3	$\mathbf{L}^{t\mathrm{Bu}}$/Ni	1	616	49	31	340	7.7
4	$\mathbf{L}^{t\mathrm{Bu}}$/Ni[c]	1	3395	162	164	1769	10.4
5	$\mathbf{L}^{t\mathrm{Bu}}$/Ni[d]	1	599	56	25	323	7.4
6	2$\mathbf{L}^{t\mathrm{Bu}}$/Ni[e]	2	647	56	20	377	8.5
7	SBA*-**L**-0.5/Ni	3	534	17	34	247	10.5
8	SBA*-**L**-1/Ni	3	377	14	22	180	10.5
9	SBA*-**L**-2/Ni	3	261	10	11	119	12.4
10	SBA*-**L**-4/Ni	3	251	10	10	117	12.6
11	SBA*-**L**-0.5/Ni[f]	3	121	16	7	83	5
12	SBA*-**L**-1/Ni[f]	3	45	4	1	30	9
13	SBA*-**L**-2/Ni[f]	3	41	2	1	22	14
14	SBA*-**L**-4/Ni[f]	3	48	6	2	31	6
15	SBA*-**L**-0.5/Ni[g]	3	282	13	7	174	14

[a] General conditions: catalyst (2 μmol), cyclohexane (15 mmol), *m*CPBA (2 mmol), CH_2Cl_2 (3 mL), MeCN (1 mL), RT. [b] Taken from reference [7]; the TONs of compound **5** in runs 1 and 2 were estimated to be about 300. [c] Catalyst (0.2 μmol). [d] With the addition of SBA*-**L**-4 (6 mg, 2 μmol of the immobilized ligand). [e] This system required a longer reaction time for the saturation of product formation. [f] Reused after washing the recovered catalyst with MeOH. [g] Reused after washing the recovered catalyst with CH_2Cl_2.

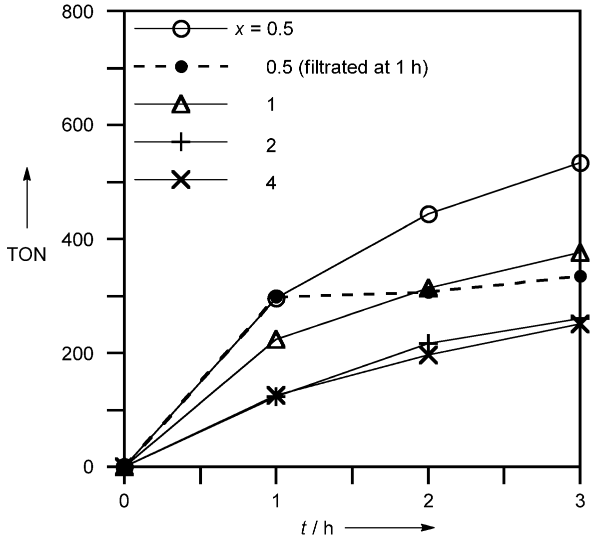

Figure 5. Progress of cyclohexanol formation in the oxidation of cyclohexane catalyzed by SBA*-**L**-*x*/Ni under standard conditions (*x* = 0.5: ○, 1: △, 2: +, 4: X) and the filtration test (*x* = 0.5 filtered at *t* = 1 h: ●, dashed line).

The relationship between catalytic activity and surface environment has been investigated (Table 4, entries 5, 7–10). The addition of SBA*-**L**-4 to the homogeneous $\mathbf{L}^{t\mathrm{Bu}}$/Ni catalysis does not cause a loss of activity (Table 4, entry 5). This result indicates that the functionalities (Si–OH, Si–O–$SiMe_3$) and the extra ligand (1 equiv for Ni) on the silica support have no significant effect on the catalysis. In heterogeneous catalysis, the yield and selectivity of compound **2** decrease upon an increase in the ligand loading (*x*) of the immobilized catalyst (Table 4, entries 7–10). This de-activation effect upon the increase in ligand loading might be correlated with the formation of the [Ni$\mathbf{L}_2$] site at higher ligand densities on the support surface. In contrast to the homogeneous 2$\mathbf{L}^{t\mathrm{Bu}}$/Ni catalyst, which shows catalytic reactivity owing to smooth ligand dissociation, the two closely fixed Py_2N sites on the solid support may act as a hexadentate chelate and force the formation of an "inert [Ni$\mathbf{L}_2$]" site. By using our facile method for loading control with high reproducibility, we have successfully observed a relationship between the reactivity and the structure of the active site on the surface in this catalyst system.

To confirm that the catalyst was reusable, the nickel loading in the recovered catalysts was analyzed by atomic absorption spectrometry after filtration of the reaction mixture and subsequent washing of the recovered catalysts with MeOH (Table 3). Lower ligand loadings in SBA*-**L**-*x*/Ni systems (*x* = 0.5, 1, and 2) show significant metal leaching, whereas the material with the highest ligand loading (*x* = 4) almost maintains its initial metal loading at a **L**/Ni ratio of 2:1. This result also supports the conclusion that the coordination equilibrium shifts toward the formation of [Ni$\mathbf{L}_2$] species upon increasing the amount of ligand on the silica surface. Metal leaching was partially suppressed by using CH_2Cl_2, which is a typical unpolar and uncoordinating solvent for Ni^{II} or Ni^{III}, instead of MeOH in the washing process during the recovery of the catalysts (initial SBA*-**L**-0.5/Ni: $Ni = 0.08\ mmol\,g^{-1}$, recovered catalyst: $Ni = 0.06$ (CH_2Cl_2) and 0.03 (MeOH) $mmol\,g^{-1}$; Table 3 and Table 4, entries 7, 11, and 15). This result suggests that the metal leaching is enhanced by protic and polar solvents during washing in the presence of the products, such as cyclohexanol and *m*-chlorobenzoic acid, with some contribution from ligand loss through oxidative decomposition. The replacement of the reaction solvent ($MeCN/CH_2Cl_2$ with CH_2Cl_2) in addition to that of the washing solvent did not further improve nickel leaching ($0.06\ mmol\,g^{-1}$).

A catalyst-reuse experiment was performed with the recovered catalysts. Owing to the loss of material and nickel leaching during the filtration step, the scale of the reaction was decreased based on the quantity of recovered nickel ions to maintain the same concentrations and ratios of reagents as in the initial run. The results were normalized to the TON. The results for the catalysts that were recovered by washing with MeOH (entries 11–14) or CH_2Cl_2 (entry 15) are shown in Table 4. The MeOH-recovered catalysts showed no activity, although some nickel ions remained. In contrast, the CH_2Cl_2-recovered SBA*-**L**-0.5/Ni catalyst exhibited some reactivity. The reuse run also indicated that nickel ions were easily displaced from the reactive $[Ni\mathbf{L}(X)_n]$ species under polar conditions, whereas any inactive nickel species remained on the catalyst support. The real deactivation process remains unknown.

Conclusions

In summary, polypyridylamine-type ligand **L** has been immobilized onto silica supports with various surface densities. By using our facile ligand-immobilization method, with controlled loading and high reproducibility, we have observed the relationship between the reactivity and structure of the active sites on the support surface. In addition, two related homogeneous model complexes, $[Ni(\mathbf{L}^{tBu})(OAc)_2(H_2O)]$ and $[Ni(\mathbf{L}^{tBu})_2](BF_4)_2$, have been prepared to determine the structure of the immobilized complex species. Disappointingly, the “click-to-chelate” approach was not successful in this investigation, but the triazole group could serve as a good anchor for attaching additional functionalities. Heterogeneous nickel SBA*-**L**-*x*/Ni catalysts retained the activity of homogeneous analogue $\mathbf{L}^{tBu}$/Ni and other reported tpa/Ni systems for alkane oxidation. Increasing the ligand density (x) decreases the catalytic activity. The site-isolated conditions, which occur when the ligand loading is low, is effective for preventing unwanted interactions between the active sites, such as the formation of $[M\mathbf{L}_2]$ species as reported herein. On the other hand, $[M\mathbf{L}_2]$ species that are formed under site-dense (ligand-rich) surfaces show inert character in comparison with the related homogeneous complex. Finally, this result clearly demonstrates the importance of the interactions between the surface sites for constructing desired catalysts on solid supports.

Experimental Section

Instrumentation and Materials

Atomic absorption analysis was performed on a Shimadzu AA-6200. Elemental analysis was performed on a Perkin–Elmer CHNS/O Analyzer 2400II. MS (ESI) spectra were recorded on a JEOL JMS-T100LC “AccuTOF” mass spectrometer. GC analysis was performed on a Shimadzu GC2010 gas chromatograph with an Rtx-5 column (Restek, length = 30 m, i.d. = 0.25 mm, thickness = 0.25 μm). IR spectra were recorded on a JASCO FTIR 4200 spectrometer. NMR spectra were recorded on a JEOL ECA-500 spectrometer. UV/Vis spectra were recorded on a JASCO V650 spectrometer with a PIN-757 integrating-sphere attachment for solid reflectance. Nitrogen-sorption studies were performed at 77 K on a Micromeritics TriStar 3000. Before the adsorption experiments, the samples were degassed under reduced pressure for 3 h at 333 K. All of the commercial reagents and solvents were used as received.

Synthesis of N,N-bis(2-pyridylmethyl)-N-{(1-tert-butyl-1H-1,2,3-triazol-4-yl)methyl}amine ($\mathbf{L}^{tBu}$)

A mixture of compound **1**[6j–l] (500 mg, 2.1 mmol), $tBuN_3$[8] (500 mg, 5.0 mmol), and copper(0) powder (1 g) was stirred in 2-methyl-2-propanol (10 mL) for 24 h under a N_2 atmosphere at RT. The copper powder was removed by filtration and the solvent was then evaporated under reduced pressure. The product was purified by column chromatography on alumina (EtOAc) to give the product as a yellow solid (566 mg, 80 % yield). M.p. 90–92 °C; ^1H NMR (300 MHz, $CDCl_3$, 25 °C, TMS): $\delta = 8.52$ (d, $J(H,H) = 4.9$ Hz, 2H; Py-6), 7.64 (t (d), $J(H,H) = 7.8$, 1.7 Hz, 2H; Py-4), 7.59 (s, 1H; triazole), 7.58 (d, $J(H,H) = 7.6$ Hz, 2H; Py-3), 7.13 (m, 2H; Py-5), 3.87 (s, 2H; NCH_2Tz), 3.85 (s, 4H; NCH_2Py), 1.64 ppm (s, 9H; *t*Bu); ^{13}C NMR (75 MHz, $CDCl_3$, 25 °C, TMS): $\delta = 159.4$, 149.1, 143.6, 136.5, 123.4, 122.0, 120.0, 59.8, 59.2, 48.9, 30.1 ppm; IR (KBr): $\tilde{\nu} = 3111$, 3061, 2977, 2935, 2872, 2814, 1590, 1570, 1472, 1434, 1371, 1326, 1302, 1235, 1211, 1137, 1050, 979, 962, 898, 866, 772, 753 cm^{-1}; UV/Vis (HCl/water): λ_{max} (ε) = 263 nm (11 700 $mol^{-1}\,dm^3\,cm^{-1}$); MS (ESI^+, MeOH): $m/z = 337.12$ $[M+H^+]$; elemental analysis calcd (%) for $C_{19}H_{24}N_6$: C 67.83, H 7.19, N 24.98; found: C 67.99, H 7.40, N 25.23.

Synthesis of $[Ni(L^{tBu})(OAc)_2(H_2O)]$ ($\mathbf{L}^{tBu}$/Ni)

A solution of $\mathbf{L}^{tBu}$ (288 mg, 0.86 mmol) in MeOH (10 mL) was added to a solution of $Ni(OAc)_2{\cdot}4H_2O$ (214 mg, 0.86 mmol) in MeOH (10 mL) with stirring, after which the solvent was evaporated. The crude mixture was dissolved in CH_2Cl_2 (10 mL) and filtrated to remove the inorganic salts. *n*-Hexane (30 mL) was layered onto the solution, which was allowed to stand for 3 days to give $\mathbf{L}^{tBu}$/Ni as blue crystals (222 mg, 49 % yield). IR (KBr): $\tilde{\nu} = 3398$, 2983, 2940, 1606, 1567, 1410, 1209, 1023, 901, 771, 731, 661 cm^{-1}; UV/Vis (CH_2Cl_2): λ_{max} (ε) = 608 (14), 771 (4), 1005 nm (14 $mol^{-1}\,dm^3\,cm^{-1}$); MS (ESI^+, MeCN): $m/z = 453.13$ $[Ni(OAc)(\mathbf{L}^{tBu})]^+$; elemental analysis calcd (%) for $[Ni(OAc)_2(H_2O)(\mathbf{L}^{tBu})]{\cdot}0.5H_2O$: C 49.20, H 5.80, N 14.65; found: C 49.31, H 5.62, N 14.82.

Synthesis of $[Ni(L^{tBu})_2](BF_4)_2$ ($2\mathbf{L}^{tBu}$/Ni)

Purple crystals of the title complex (340 mg, 72 % yield) were obtained after several days by the slow diffusion of a solution of $\mathbf{L}^{tBu}$ (370 mg, 1.1 mmol) in EtOH (3 mL) into a solution of $Ni(BF_4){\cdot}6H_2O$ (170 mg, 0.5 mmol) in EtOH (6 mL) in a test tube. The crystal was corrected by filtration and washed with EtOH. Instead of the slow-diffusion procedure, rapid mixing of the two solutions gave the title complex as a purple powder within 30 min. IR (KBr): $\tilde{\nu} = 3161$, 3077, 2984, 2936, 1610, 1450, 1054, 770, 758 cm^{-1}; UV/Vis (CH_2Cl_2): λ_{max} (ε) = 568 (23), 818 (8), 973 nm (19 $mol^{-1}\,dm^3\,cm^{-1}$); MS (ESI^+, MeCN): $m/z = 817.29$ $[Ni(\mathbf{L}^{tBu})_2(BF_4)]^+$; elemental analysis calcd (%) for $[Ni(\mathbf{L}^{tBu})_2](BF_4)_2{\cdot}2H_2O$: C 48.49, H 5.57, N 17.86; found: C 48.45, H 5.30, N 17.83.

*Preparation of SBA-**L**-x: General Procedure for Click Attachment*

The starting material, SBA-N_3-*x* ($x = 0.5$, 1, 2, 4), was prepared according to a literature procedure.[3] A suspension of SBA-N_3-*x* (1.0 g) in DMF (100 mL), *N*-propargyl-*N*,*N*-bis(2-pyridylmethyl)amine (about 2 equiv for N_3 loading), and copper(II) sulfate (about 2 equiv for N_3 loading) was degassed under a flow of Ar for 30 min at RT. Then, sodium ascorbate (5 equiv for N_3 loading in 5 mL water) was added to the suspension and the mixture was stirred for 24 h under an Ar atmosphere. The silica was recovered by filtration and washed with DMF and water. To remove the copper catalyst, the silica was repeatedly washed with a solution of sodium *N*,*N*-diethyldithiocarbamate (Na-ddtc, 0.1 $mol^{-1} dm^3$) in MeOH, DMF, and MeOH until the brownish color of the silica had disappeared. Finally, the silica was rinsed with a solution of sodium acetate (0.01 $mol^{-1} dm^3$) in MeOH and in MeOH, before being vacuum-dried at RT for 24 h to yield SBA-**L**-*x*.

Preparation of SBA-**L**-x: General Procedure for End-Capping with trimethylsilyl (TMS) Groups*

SBA-**L**-*x* (0.8 g) was suspended in toluene (50 mL) under an Ar atmosphere. Then, the suspension was heated at 50 °C with 1,1,1,3,3,3-hexamethyldisilazane (HMDS, 0.37 mL, 1.7 mmol) for 1 h and the silica was recovered by membrane filtration. The silica was washed with toluene and vacuum-dried at RT for 24 h to give end-capped silica SBA*-**L**-*x* as a pale-yellow powder.

General Procedure for the Preparation of SBA-**L**-x/Ni*

SBA*-**L**-*x* (0.5 g) was suspended into a solution of $Ni(OAc)_2{\cdot}4H_2O$ (1.5 equiv for ligand) in MeOH (50 mL) and the mixture was stirred for 30 min. The silica powder was recovered by membrane filtration, washed with MeOH, and vacuum-dried at RT for 24 h to give SBA*-**L**-*x*/Ni.

Crystallography

The preparation of single crystals of complexes $\mathbf{L}^{t\mathrm{Bu}}$/Ni and 2$\mathbf{L}^{t\mathrm{Bu}}$/Ni was discussed in the synthesis section. Diffraction data for all single crystals were collected on a Rigaku Saturn 70 CDD area-detector system with graphite-monochromated $Mo_{K\alpha}$ radiation. Crystals were mounted onto loops with liquid paraffin and then flash cooled to 113 K. Data collection and processing were performed by using Rigaku CrystalClear software.[16] Structural solution was performed by using direct methods (SIR-92[17]) and refinements were performed by using full-matrix least-squares (SHELXL-97[18]) against F^2; all reflections were performed by using WinGX software.[19] For complex 2$\mathbf{L}^{t\mathrm{Bu}}$/Ni, racemic twin refinement was applied by using SHELEX-97. All nonhydrogen atoms were refined anisotropically. Hydrogen atoms that were adjacent to carbon atoms were placed at calculated positions. Hydrogen atoms on oxygen atoms were located by using difference Fourier synthesis and were refined isotropically. The molecular structures were visualized by using the ORTEP-3 program.[20] Crystallographic data are summarized in Table 5. CCDC 860009 ($\mathbf{L}^{t\mathrm{Bu}}$/Ni) and CCDC 860010 (2$\mathbf{L}^{t\mathrm{Bu}}$/Ni) contain the supplementary crystallographic data for this paper. These data can be obtained free of charge from The Cambridge Crystallographic Data Centre via www.ccdc.cam.ac.uk/data_request/cif.

Quantification of the Loadings of the Immobilized Ligand and Nickel

The procedure for the determination of the ligand loadings of SBA-**L**-*x* was as follows: SBA-**L**-*x* (5 mg) was dissolved in an aqueous solution of potassium hydroxide (10 %, 1 mL) and the mixture was boiled for 5 min. Then, the solution was diluted with an aqueous solution of HCl (about 0.1 $mol^{-1} dm^3$) to a total volume of 100 mL and a UV/Vis spectrum was recorded in a cell (path length: 1 cm). The ligand loading was calculated by using the homogeneous analogue, $\mathbf{L}^{t\mathrm{Bu}}$ ($\lambda = 263$ nm, $\varepsilon = 11\,700\ mol^{-1} dm^3 cm^{-1}$ in aqueous HCl), as a reference.

The procedure for determining the ligand loadings of SBA*-**L**-*x* was as follows: SBA*-**L**-*x* (5 mg) and acidic NH_4F (18 mg) were dissolved in MeOH (5 mL) under gentle heating (50 °C) for several hours. Then, the solution was diluted with MeOH and a concentrated aqueous solution of HCl (about 1 mL) to a total volume of 100 mL and a UV/Vis spectrum was recorded in a cell (path length: 1 cm). The ligand loading was calculated by using the homogeneous analogue, $\mathbf{L}^{t\mathrm{Bu}}$ ($\lambda = 263$ nm, $\varepsilon = 11\,700\ mol^{-1} dm^3 cm^{-1}$ in aqueous HCl), as a reference.

Table 5. Crystallographic data of complexes $\mathbf{L}^{t\mathrm{Bu}}$/Ni and 2$\mathbf{L}^{t\mathrm{Bu}}$/Ni.

	$\mathbf{L}^{t\mathrm{Bu}}$/Ni	2$\mathbf{L}^{t\mathrm{Bu}}$/Ni
formula	$C_{23}H_{32}N_6NiO_5{\cdot}CH_2Cl_2$	$C_{38}H_{48}B_2F_8N_{12}Ni{\cdot}(H_2O)_{1.5}$
M_w	616.18	932.24
crystal color, shape	blue, block	purple, platelet
crystal size [mm]	0.2 × 0.3 × 0.4	0.15 × 0.35 × 0.45
crystal system	monoclinic	tetragonal
space group	$P2_1/n$ (#14)	$I4_122$ (#98)
a [Å]	11.913(3)	18.0581(2)
b [Å]	14.014(4)	18.0581(2)
c [Å]	34.872(9)	57.3310(11)
β [°]	92.034(3)	90
V [Å^3]	5818(3)	18 695.3(5)
Z	8	16
2θ range [°]	2.34–55.00	2.84–54.92
F(000)	2576	7760
T [K]	113	113
ρ_{calcd} [g cm^{-3}]	1.407	1.325
$\mu(Mo_{K\alpha})$ [mm^{-1}]	0.894	0.492
R, R_w ($I > 2\sigma(I)$)[a]	0.0503, 0.1283	0.0757, 0.2142
R, R_w (all data)[a]	0.0559, 0.1245	0.0769, 0.2162
GOF on S[b]	1.153	1.092

[a] $R = \Sigma||F_o| - |F_c||/\Sigma|F_o|$. $R_w = \{\Sigma[w(F_o^2 - F_c^2)^2]/\Sigma[w(F_o^2)^2]\}^{1/2}$. [b] $S = \{\Sigma[w(F_o^2 - F_c^2)^2]/(n-p)\}^{1/2}$, where n is the number of reflections and p is the total number of refined parameters.

The procedure for determining the Ni loadings of SBA*-**L**-*x*/Ni was as follows: SBA*-**L**-*x*/Ni (5 mg) was dissolved in a 10 % aqueous solution of KOH (1 mL) with heating for 5 min. Then, the solution was acidified with a concentrated aqueous solution of HNO_3 (2 mL) and diluted with water to a total volume of 10 mL. The solution was passed through a syringe filter prior to its introduction into an atomic absorption spectrometer.

Oxidation of Cyclohexane

Cyclohexane was oxidized at RT under an Ar atmosphere. In a typical reaction,[7] a solution (or suspension) of the homogeneous (or heterogeneous) nickel complex (2.0 μmol) in MeCN (1.0 mL) and CH_2Cl_2 (1.0 mL) was added to a mixture of cyclohexane (15 mmol, 1.6 mL), *m*CPBA (345 mg, 2.0 mmol), and nitrobenzene (10 μL, 100 μmol, as a GC standard) in CH_2Cl_2 (2.0 mL). To monitor the product formation, an aliquot of the reaction mixture (0.2 mL) was extracted at certain times and quenched with a solution of triphenylphosphine (10 mg) in CH_2Cl_2 (0.5 mL), after which the solution was subjected to GC analysis. The reported data are averages of three independent measurements. No change in reactivity was observed under shaking instead of mechanical stirring with a Teflon-coated magnetic stirrer bar.

Acknowledgements

This work was supported by a Grant in-Aid for Scientific Research (20360367), the Cooperative Research Program of the Network Joint Research Center for Materials and Devices (2011169, 2012216, and 2012348), the Strategic Development of Research Infrastructure for Private Universities and a Scientific Frontier Research Project from the Ministry of Education, Culture, Sports, Science, and Technology of Japan, and by the Stanford Global Climate and Energy Project (GCEP).

---

[1] a) D. E. De Vos, M. Dams, B. F. Sels, P. A. Jacobs, *Chem. Rev.* **2002**, *102*, 3615–3640; b) Q.-H. Xia, H.-Q. Ge, C.-P. Ye, Z.-M. Liu, K.-X. Su, *Chem. Rev.* **2005**, *105*, 1603–1662; c) E. Brulé, Y. R. de Miguel,

Org. Biomol. Chem. **2006**, *4*, 599–609; d) S. Minakata, M. Komatsu, *Chem. Rev.* **2009**, *109*, 711–724; e) A. Zamboulis, N. Moitra, J. J. E. Moreau, X. Cattöen, M. W. C. Man, *J. Mater. Chem.* **2010**, *20*, 9322–9338; f) S. Shylesh, M. J. Jia, W. R. Thiel, *Eur. J. Inorg. Chem.* **2010**, 4395–4410; g) C. W. Jones, *Top. Catal.* **2010**, *53*, 942–952.

[2] a) M. Tada, T. Taniike, L. M. Kantam, Y. Iwasawa, *Chem. Commun.* **2004**, 2542–2543; b) J. C. Hicks, R. Dabestani, A. C. Buchanan, C. W. Jones, *Chem. Mater.* **2006**, *18*, 5022–5032; c) J. C. Hicks, C. W. Jones, *Langmuir* **2006**, *22*, 2676–2681; d) M. Tada, R. Coquet, J. Yoshida, M. Kinoshita, Y. Iwasawa, *Angew. Chem.* **2007**, *119*, 7358–7361; *Angew. Chem. Int. Ed.* **2007**, *46*, 7220–7223; e) K. Cheng, C. C. Landry, *J. Am. Chem. Soc.* **2007**, *129*, 9674–9685; f) G. Grigoropoulou, K. C. Christoforidis, M. Louloudi, Y. Deligiannakis, *Langmuir* **2007**, *23*, 10407–10418; g) T. J. Terry, G. Dubois, A. Murphy, T. D. P. Stack, *Angew. Chem.* **2007**, *119*, 963–965; *Angew. Chem. Int. Ed.* **2007**, *46*, 945–947; h) T. J. Terry, T. D. P. Stack, *J. Am. Chem. Soc.* **2008**, *130*, 4945–4953; i) J. M. Fraile, J. I. García, C. I. Herrerías, J. A. Mayoral, E. Pires, *Chem. Soc. Rev.* **2009**, *38*, 695–706; j) J. M. Fraile, J. I. García, J. A. Mayoral, *Chem. Rev.* **2009**, *109*, 360–417.

[3] a) J. Nakazawa, T. D. P. Stack, *J. Am. Chem. Soc.* **2008**, *130*, 14360–14361; b) J. Nakazawa, B. J. Smith, T. D. P. Stack, *J. Am. Chem. Soc.* **2012**, *134*, 2750–2759.

[4] a) D. J. Macquarrie, *Chem. Commun.* **1996**, 1961–1962; b) S. Huh, J. W. Wiench, J.-C. Yoo, M. Pruski, V. S.-Y. Lin, *Chem. Mater.* **2003**, *15*, 4247–4256; c) V. Matsura, Y. Guari, J. Larionova, C. Guérin, A. Caneschi, C. Sangregorio, E. Lancelle-Beltran, A. Mehdi, R. J. P. Corriu, *J. Mater. Chem.* **2004**, *14*, 3026–3033; d) R. J. P. Corriu, A. Mehdi, C. Reyé, C. Thieuleux, *Chem. Mater.* **2004**, *16*, 159–166; e) J. Alauzun, A. Mehdi, C. Reyé, R. Corriu, *New J. Chem.* **2007**, *31*, 911–915; f) C.-T. Tsai, Y.-C. Pan, C.-C. Ting, S. Vetrivel, A. S. T. Chiang, G. T. K. Fey, H.-M. Kao, *Chem. Commun.* **2009**, 5018–5020.

[5] D. Y. Zhao, J. L. Feng, Q. S. Huo, N. Melosh, G. H. Fredrickson, B. F. Chmelka, G. D. Stucky, *Science* **1998**, *279*, 548–552.

[6] a) V. V. Rostovtsev, L. G. Green, V. V. Fokin, K. B. Sharpless, *Angew. Chem.* **2002**, *114*, 2708–2711; *Angew. Chem. Int. Ed.* **2002**, *41*, 2596–2599; b) V. O. Rodionov, S. I. Presolski, D. D. Diaz, V. V. Fokin, M. G. Finn, *J. Am. Chem. Soc.* **2007**, *129*, 12705–12712; c) W. H. Binder, C. Kluger, *Curr. Org. Chem.* **2006**, *10*, 1791–1815; d) Z. M. Guo, A. W. Lei, X. M. Liang, Q. Xu, *Chem. Commun.* **2006**, 4512–4514; e) M. Ortega-Muñoz, J. Lopez-Jaramillo, F. Hernandez-Mateo, F. Santoyo-Gonzalez, *Adv. Synth. Catal.* **2006**, *348*, 2410–2420; f) J. P. Collman, N. K. Devaraj, T. P. A. Eberspacher, C. E. D. Chidsey, *Langmuir* **2006**, *22*, 2457–2464; g) J. P. Collman, L. Zeng, H. J. H. Wang, A. Lei, J. I. Brauman, *Eur. J. Org. Chem.* **2006**, 2707–2714; h) A. Devadoss, C. E. D. Chidsey, *J. Am. Chem. Soc.* **2007**, *129*, 5370–5371; i) D. E. Bergbreiter, P. N. Hamilton, N. M. Koshti, *J. Am. Chem. Soc.* **2007**, *129*, 10666–10667; j) S. Huang, R. J. Clark, L. Zhu, *Org. Lett.* **2007**, *9*, 4999–5002; k) H. A. Michaels, C. S. Murphy, R. J. Clark, M. W. Davidson, L. Zhu, *Inorg. Chem.* **2010**, *49*, 4278–4287; l) J. Rosenthal, S. J. Lippard, *J. Am. Chem. Soc.* **2010**, *132*, 5536–5537; m) J. M. Lee, J. Kim, Y. Shin, C. E. Yeom, J. E. Lee, T. Hyeon, B. M. Kim, *Tetrahedron: Asymmetry* **2010**, *21*, 285–291; n) B. S. Rana, S. L. Jain, B. Singh, A. Bhaumik, B. Sain, A. K. Sinha, *Dalton Trans.* **2010**, *39*, 7760–7767; o) C. M. Fu, H. Y. Shi, G. S. Qian, Z. W. Li, *Chin. Chem. Lett.* **2009**, *20*, 1345–1347; p) T. L. Mindt, H. Struthers, B. Spingler, L. Brans, D. Tourwé, E. García-Garayoa, R. Schibli, *ChemMedChem* **2010**, *5*, 2026–2038; q) G. Zhang, Y. Wang, X. Wen, C. Ding, Y. Li, *Chem. Commun.* **2012**, *48*, 2979–2981.

[7] a) T. Nagataki, Y. Tachi, S. Itoh, *Chem. Commun.* **2006**, 4016–4018; b) T. Nagataki, K. Ishii, Y. Tachi, S. Itoh, *Dalton Trans.* **2007**, 1120–1128; c) T. Nagataki, S. Itoh, *Chem. Lett.* **2007**, *36*, 748–749.

[8] J. C. Bottaro, P. E. Penwell, R. J. Schmitt, *Synth. Commun.* **1997**, *27*, 1465–1467.

[9] a) D. Schweinfurth, R. Pattacini, S. Strobel, B. Sarkar, *Dalton Trans.* **2009**, 9291–9297; b) M. Ostermeier, M.-A. Berlin, R. M. Meudtner, S. Demeshko, F. Meyer, C. Limberg, S. Hecht, *Chem. Eur. J.* **2010**, *16*, 10202–10213; c) O. Fleischel, N. Wu, A. Petitjean, *Chem. Commun.* **2010**, *46*, 8454–8456; d) S. Zanarini, M. Felici, G. Valenti, M. Marcaccio, L. Prodi, S. Bonacchi, P. Contreras-Carballada, R. M. Williams, M. C. Feiters, R. J. M. Nolte, L. De Cola, F. Paolucci, *Chem. Eur. J.* **2011**, *17*, 4640–4647; e) C. H. Zhang, X. D. Shen, R. Sakai, M. Gottschaldt, U. S. Schubert, S. Hirohara, M. Tanihara, S. Yano, M. Obata, N. O. Xiao, T. Satoh, T. Kakuchi, *J. Polym. Sci. Part A* **2011**, *49*, 746–753.

[10] J. P. Wikstrom, A. S. Filatov, R. J. Staples, C. R. Guifarro, E. V. Rybak-Akimova, *Inorg. Chim. Acta* **2010**, *363*, 884–890.

[11] S. Brunauer, P. H. Emmett, E. Teller, *J. Am. Chem. Soc.* **1938**, *60*, 309–319.

[12] E. P. Barrett, L. G. Joyner, P. P. Halenda, *J. Am. Chem. Soc.* **1951**, *73*, 373–380.

[13] G. Türkoglu, C. P. Ulldemolins, R. Müller, E. Hübner, F. W. Heinemann, M. Wolf, N. Burzlaff, *Eur. J. Inorg. Chem.* **2010**, 2962–2974.

[14] a) M. Ghorbanloo, H. H. Monfared, C. Janiak, *J. Mol. Catal. A* **2011**, *345*, 12–20; b) M. Weck, C. W. Jones, *Inorg. Chem.* **2007**, *46*, 1865–1875.

[15] W. Nam, J. Y. Ryu, I. Kim, C. Kim, *Tetrahedron Lett.* **2002**, *43*, 5487–5490.

[16] Rigaku corporation, **1999**.

[17] A. Altomare, G. Cascarano, C. Giacovazzo, A. Guagliardi, *J. Appl. Crystallogr.* **1993**, *26*, 343–350.

[18] G. M. Sheldrick, *Acta Crystallogr. Sect. A* **2008**, *64*, 123–134.

[19] L. J. Farrugia, *J. Appl. Crystallogr.* **1999**, *32*, 837–838.

[20] L. J. Farrugia, *J. Appl. Crystallogr.* **1997**, *30*, 565.

Received: February 6, 2013

Heterogeneous Catalysis

Jun Nakazawa, Tomoaki Hori,*
T. Daniel P. Stack,
*Shiro Hikichi** ________ ■■■■–■■■■

Alkane Oxidation by an Immobilized Nickel Complex Catalyst: Structural and Reactivity Differences Induced by Surface-Ligand Density on Mesoporous Silica

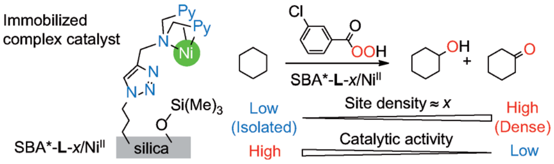

Going nowhere fast: An immobilized SBA*-**L**-*x*/Ni complex was prepared with various ligand loadings and used in the oxidation of cyclohexane. The importance of site-density control for the development of immobilized catalysts has been demonstrated.